Performance Assessment of PIT VIPER Cables Following Long-duration Solder Exposure During Manufacturing

Amy Watterson, Amanda Hubbard, Rui Diaz-Pacheco, Ashleigh Francis, Robert Granetz, James Logan, Theodore Golfinopoulos, Alexey Kaplan, Philip Michael, Richard Murray, Charlie Sanabria, Shane Schweiger, Thomas Toland, Rui Vieira

***Abstract*—PIT VIPER cables are rare-earth barium copper oxide (REBCO)-based high-temperature superconducting (HTS) cables developed at the Massachusetts Institute of Technology and Commonwealth Fusion Systems. The cable design consists of a twisted copper former with grooves filled with stacks of REBCO tape, enclosed in a structural jacket. The assembly is then filled with solder in a vacuum pressure impregnation (VPI) process. One side effect of the VPI process, however, is potential damage to the superconductor that reduces its critical current and critical exponent. Damage may result from two mechanisms: prolonged exposure to elevated temperatures, and physical erosion of the copper stabilizer layer of the HTS tape, which leaves parts of the REBCO layer unprotected. In this experiment, the effect of extended time scales (> 2 hours) of flowing tin-lead-based solder exposure on HTS in PIT VIPER cables was tested, exploring for the first time exposure to flowing solder at a time scale that is particularly relevant to large-scale magnet manufacturing. During this study, two experimental samples were manufactured for electrical testing: one 2.5-meter-long straight cable, and one 20-meter-long coiled cable. Each cable was exposed to molten tin-lead solder for 2.5 hours during the VPI process and then electrically tested in a liquid nitrogen bath. Critical current, n-value, and resistance were measured. Critical current is compared to modeled values determined from characterization of the tape used, and degradation is assessed from this comparison. The measured critical current, when tested in a liquid nitrogen bath and under self-field, was uniform within reasonable experimental error. This result de-risks solder degradation for the manufacturing of SPARC cable magnets.**

***Index Terms*—Fusion magnets, HTS magnets, Superconducting magnets.**

I. Introduction

PIT VIPER superconducting cables [1], [2] (Fig. 1) have been developed jointly by the Massachusetts Institute of Technology Plasma Science and Fusion Center (MIT PSFC) and Commonwealth Fusion Systems (CFS) for use as part of the SPARC tokamak's magnet system [3]. Manufacture of these rare-earth barium copper oxide (REBCO) high temperature superconductor (HTS)-based cables includes a solder vacuum impregnation process [4] which involves flowing molten lead-tin solder down the length of the cable while above the melting point of solder.

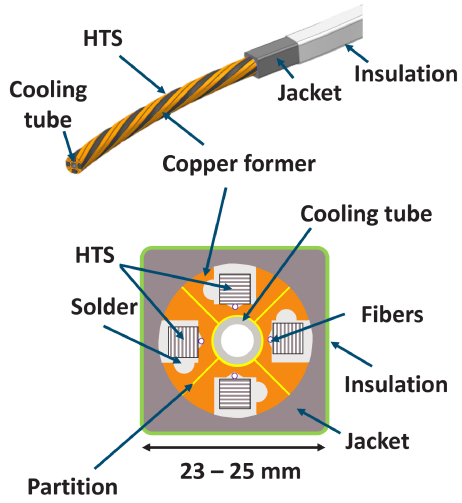

Fig. 1. Diagram of a four-petal PIT VIPER cable.

Two major identified risks related to cable soldering are discussed. Firstly, there is the possibility that the superconductor will be damaged during the elevated temperature manufacturing process required to make the magnets. At these temperatures, there is a risk of I_c degradation caused by oxygen out-diffusion from the REBCO layer [5], [6].

The second major risk is the erosion of the stabilizing copper of the REBCO tapes due to its solubility in tin-lead. Cross-sectional images of previously tested VIPER and PIT VIPER cables have revealed that the protective copper stabilizer coating on REBCO HTS is eroded away by forming Cu-Sn intermetallic. One such picture from a cable tested at the SULTAN facility is shown in Fig. 2. This erosion leaves the part of the thin REBCO layer unprotected and potentially at risk to damage.

II. Motivation

The motivation of this paper is to estimate the time scale associated with solder manufacturing at scales relevant for SPARC, and then to test for and quantify the resulting potential damage. The longest cables needed for the SPARC poloidal field coil will be on the order of several hundred meters in

This work was primarily funded by Commonwealth Fusion Systems and partially funded by ARPA-E Award Number DE-AR0001259.

Amy Watterson, Amanda Hubbard, Robert Granetz, Theodore Golfinopoulos, Alexey Kaplan, Philip Michael, Richard Murray, Shane Schweiger, Thomas Toland, and Rui Vieira are with the MIT Plasma Science and Fusion Center, Cambridge, MA 02139 USA (e-mail: watterson@psfc.mit.edu).

Rui Diaz-Pacheco, Ashleigh Francis, James Logan, and Charlie Sanabria are with Commonwealth Fusion Systems, Devens, MA 01434 USA.

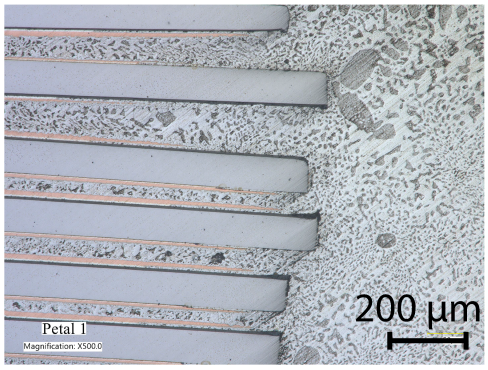

Fig. 2. Micrograph of HTS tapes after solder erosion, showing missing copper stabilizer.

length. In order to solder a cable of this length, the cable must be held at elevated temperature above solder melting point for the duration of the flow from inlet to outlet. This process takes hours to complete. In this experiment both heat treatment and solder erosion at large scale in real manufacturing conditions were tested. Two sample articles were fabricated and electrically tested in liquid nitrogen at self-field: one 20-meter-long coil and one 2.5-meter-long straight cable.

III. Solder Flow Model

To determine how long solder will take to fill the longest cables required for SPARC, a fluid model was developed based on experimental data gathered during multiple solder runs and extrapolated to large scale. The solder flowing through a closed cable may be described by physical laws. The Darcy-Weisbach equation (equation 1) best describes the pressure-driven flow in our experimental database, in which Δp is the pressure drop, l is the flow length, f_D is the Darcy friction factor, ρ is the density of the fluid, v is the fluid velocity, and D_H is the hydraulic diameter.

$$\frac{\Delta p}{l} = f_D \cdot \frac{\rho}{2} \cdot \frac{\langle v \rangle^2}{D_H} \tag{1}$$

The flow down a cable is assumed to be simple pressure driven flow because of a small channel cut into the copper former. Solder primarily flows down this channel while some amount of the flow is diverted to fill around the tape stack. [7] From equation 1, an equation that describes the flow rate of solder over time as it fills up an empty cable can be developed. The length of the cable is split up into a number of segments n of length l_{seg}. As the flow progresses down the cable, the total length it has passed through is l_n, as shown in Fig. 3. For each segment, equation 1 is solved to find the velocity v_n at each given l_n. The total time can then be summed as in equation 2.

$$time_{total} = \sum_{1}^{N} \frac{l_{seg}}{v_n} \tag{2}$$

Next, equations 1 and 2 are used in conjunction to solve the time it would take to fill a cable as a function of its length. It was quickly determined these two equations alone did not well-fit experimental data. The hydraulic cross section of the solder flow area is complex and changes along the length due to relative movement of the tape stack within the channel. As a result, the hydraulic diameter, D_H, is used as a fit parameter to be determined by empirical correlation. In addition, a supplementary friction term was added to the Darcy-Weisbach equation. This term, K_{fill}, is added to account for additional flow restriction caused by anything that is not otherwise accounted for. The modified equation used for this model is thus

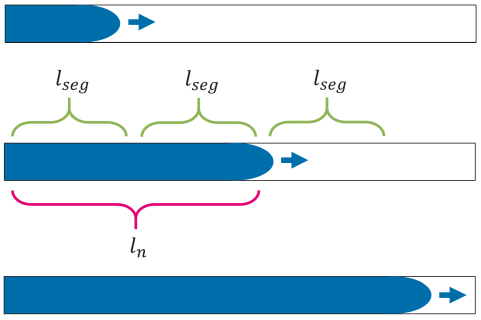

Fig. 3. Diagram showing solder flow model steps.

$$\Delta p_n = \left(f_D \frac{l_n}{D_H} + K_{fill} \right) \cdot \frac{\rho}{2} \cdot \langle v_n \rangle^2 \tag{3}$$

Equations 3 and 2 were implemented as a 1-D MATLAB function. The friction factor, f_D, correlation was used from [8], which was chosen for its smooth transition between laminar and turbulent flow regimes.

The experimental data used to fit the model was obtained from the soldering process of a 100-meter-long cable, made in July 2022 to test the SPARC HTS cable manufacturing line. During the solder process, the solder reservoir sits on a set of load cells which measure the change in weight of solder over time, or mass flow rate. In addition, liquid level switches monitor the location of the solder front in multiple locations throughout the system. Combining the data from the load cells and the level switches, the mass flow rate over time can be converted into distance over time.

MATLAB's CurveFitter module was then used to fit the two parameters, D_H and K_{fill}. The number of segments used, N, was 20. The fit results are:

$$D_H = 0.9435mm \text{ and } K_{fill} = 583.1 \tag{4}$$

The 95% confidence bounds of the fit are (0.9429, 0.9442) and (574.6, 591.6), respectively. A plot of the experimental data and extrapolation is shown in Fig. 4. Based on this analysis, 2.5 hours was chosen as a target process time that would be representative of long cables. The target terminal mass flow rate based on this time was 0.43 kg/min of solder, although exposure time was deemed a more important process target for the most representative solder erosion.

IV. Test Cable Design and Solder Process

Two cables were manufactured for this experiment: one 2.5-meter-long straight cable and one 20-meter-long coiled cable. Both cables are made of five-petal PIT VIPER, which

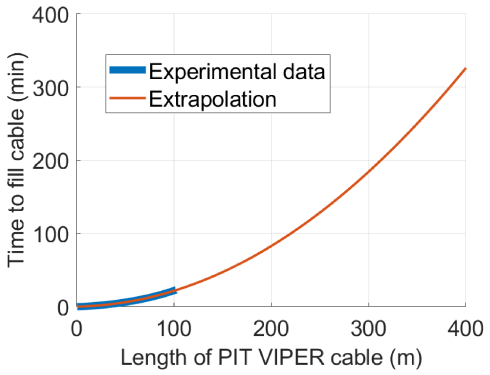

Fig. 4. Experimental flow data plotted over solder flow model extrapolation.

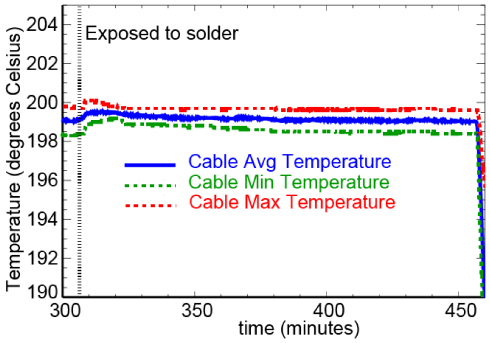

Fig. 5. Process temperatures of coil during soldering.

will be used for SPARC's poloidal field cables. One petal contained 51 HTS tapes in the straight cable, and 53 tapes in the coiled cable, while the other four petals contained non-superconductive filler tape. The cables were manufactured at the CFS facility and then solder VPI was carried out at MIT.

In order to simulate the long solder process of a cable several hundred meters in length without actually manufacturing one, a thin copper tube is added to the end of the cable to increase pressure drop and slow down flow. Both cables had a 15.2 m-long coiled copper tube with an inner radius of 1.5 mm connected to the outlet of the cable. The solder flow speed is low enough that the major radius of the coiled copper tube has negligible effects on flow and is neglected. Similarly, the major radius of the coiled PIT VIPER cable is neglected for flow calculations.

The solder process consists of heating up the cable to above solder melting temperature, and then flowing solder through the cable while at temperature. Fig. 5 shows the temperature of the PIT VIPER coil while solder flowed.

The cables were held between 198-200° Celsius for the entire 2.5 hours solder exposure. The assembly saw a steady flow rate of 0.84 kg/min after exiting the cable and coiled tube, and a total of 33 kg of solder through the sample. Flow was stopped after 45 minutes. The straight cable saw a steady exit flow rate of 0.29 kg/min, and a total of 4.8 kg of solder through the sample. Flow stalled due to unrelated facility problems after 25 minutes. Both cables were then held at temperature for the remainder of the 150 minutes of molten solder exposure time.

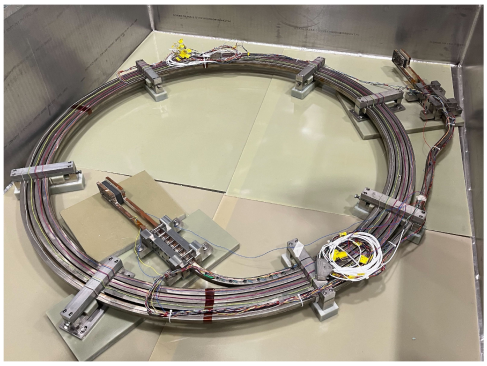

Fig. 6. Instrumented coil in dry cryobath.

V. Electrical Test Setup

Both cables were electrically tested in liquid nitrogen baths at MIT [9]. Voltage taps were attached to the cables with multiple methods. During previous test campaigns, we have observed that the voltage measured on the outside of the jacket is not always identical to that of the underlying superconductor. Thus, for the straight cable, sections of the stainless steel jacket were removed, and taps were soldered directly onto the copper former. On the coil, holes were drilled through the jacket, and wires were attached to the soldered former through nylon screws. These methods were used to keep the voltage of the jacket from distorting the underlying cable voltage signals. Additionally, several redundant taps were spot-welded to the jacket for comparison. Measured voltages are accurate within 1 μV, and measured current readings are accurate within 0.2%.

The cables were connected to a 16 kA, 10 V Magna-Power power supply through water-cooled bus cables and then superconducting bus leads. The cryobaths were filled with liquid nitrogen with a level detector and automatic fill control, ensuring that the samples were fully submerged at all times.

A Lake Shore Cernox CX-1080 temperature sensor was used to monitor the temperature of the liquid nitrogen bath, which varies slightly with atmospheric pressure. The critical current model was then scaled based on the sensor reading.

To obtain performance data, current was ramped through the cables in a series of steps. Each cable was tested individually. To eliminate the $\frac{dI}{dt}$ transient response from the parametric fit to the voltage data, equation 5, a stairstep-shaped current pattern is used, shown in Fig. 7. This results in a series of data points where $\frac{dI}{dt} = 0$. Fig. 8a shows the corresponding V-I curve. The experimental data includes ramp-up regions, where the voltage increases sharply due to inductance of the coil. Each colored flat top in Fig. 7 corresponds to the same-colored data point in Fig. 8a.

The equation used to fit voltage data is shown in equation 5, where $V_{crit} = \ell \times 1\frac{\mu V}{\mathrm{cm}}$, where ℓ is the distance between the voltage taps.

$$V = V_{crit}\left(\frac{I}{I_c}\right)^n + IR \tag{5}$$

Representative V-I fits for each cable are shown in Fig. 8a and 8b. The results from fits are shown in Table I. Each cable had multiple pairs of voltage taps, both close and far apart.

TABLE I
RESULTS SUMMARY

Sample	Modeled critical current (CFS model)	Modeled critical current (PSFC model)	Mean experimental critical current	Mean % difference	n-value
Straight	3222 A	3260 A	3217 A ±3%	-0.16%,-1.3%	20.8
Coil	3162 A	(not calculated)	3242 A ±3%	+2.5%	22.8

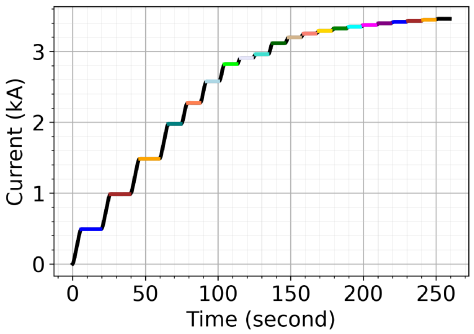

Fig. 7. Current ramp with color-coded flat tops (coil test.)

The voltage taps on the straight cable were connected only to the superconducting petal. The taps on the coiled cable were not perfectly aligned to the superconducting petal. As a result, the voltage tap pairs on the straight cable had very good precision, with a spread of 150 A between the highest and lowest calculated critical current. Because of the resistive partitions between the segmented petals (shown in Fig. 1), the short-distance taps on coiled cable had additional voltage patterns associated with measurement across and between non-superconducting petals, and as such the critical currents from the joint regions have not been included. Instead, only the turn-to-turn taps were considered, which had a spread of 67 A critical current. Typical values from experiments run over separate days have agreed within 3%.

VI. CRITICAL CURRENT MODEL

In order to quantify performance degradation, a way to compare the as-manufactured cable to an ideal, perfect cable is needed. Solder-impregnated cables cannot be electrically tested before soldering, and therefore models are used to estimate the ideal performance. Two models are employed for this experiment, one developed by MIT PSFC [10] and one by CFS. The models have been refined over several years of sample testing [11], [9], [12]. The two models are used for redundancy and to cross-check results. The discrepancy between the ideal model estimate for I_c and the measured value is used as a surrogate for degradation. Here, the degradation value obtained describes the degradation of the entire SPARC manufacturing line, including tape insertion and bending.

For input to the model, a Tapestar [13] measurement is taken on each reel in the stack and scaled to the measured I_c (77 K, self-field) taken by transport measurement on a known location of the tape. The length-averaged I_c (77 K, self-field) for each reel is then calculated from the Tapestar data and scaled to an averaged $I_c(B, T, \theta)$ dataset created from high resolution I_c measurements on multiple reels using a SuperCurrent [14] measurement system. All tape transport measurements used a $1\frac{\mu V}{cm}$ electric field criterion to determine I_c [15]. In addition, the coiled cable was 3D scanned to obtain a precise measurement of the tape path. This path was

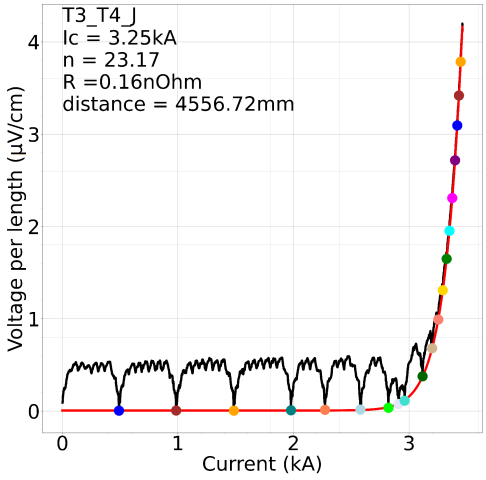

(a) Coil data, with color coded flat top data points.

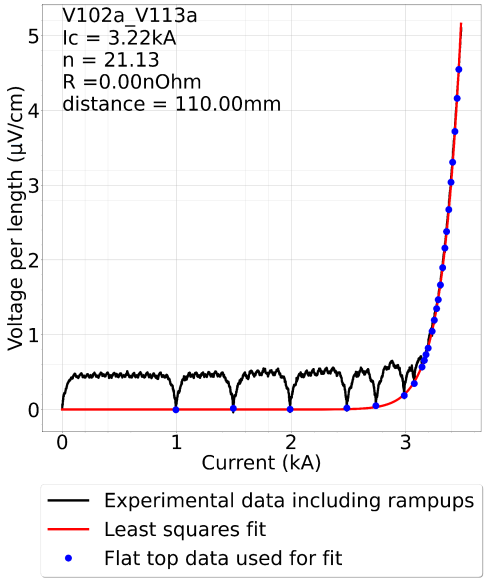

(b) Straight cable data.

Fig. 8. V-I curve and regression results from the middle of each cable.

implemented only in the CFS critical current model. The tapes used are representative SPARC HTS tapes.

The PSFC model is implemented as follows: a uniform current is initially assigned to all the filaments. The self-generated B-field and its angle to the tape surface, θ, is calculated at every filament in the cable at the desired cross-section using Biot-Savart. Given B and θ, the I_c for each grid point on each filament is interpolated from the tape databases described in the previous paragraph. Using these updated currents, the next iteration proceeds. A new set of B-fields and angles are computed, and then interpolation from the table provides the 2nd iteration of currents. This iterative process continues until the current distribution converges. Once converged, the I_c at the chosen location is the sum of the currents in all the filaments. The CFS model follows a similar method with slightly different implementation. The results from these models as well as experimental results are shown in Table I. A more detailed description of these models can be found in [1].

VII. Conclusion

The impact of long-duration solder processes on HTS cable manufacturing was explored in this study. Two samples, a straight cable and a coiled cable, were exposed to a vacuum-impregnation solder process for 2.5 hours. The manufacturing process for SPARC requires a duration of this order. All results are summarized in Table I. The measured critical current of the straight cable was at most 1.3% lower than modeled value, and the measured I_c of the coil was 2.5% higher than the modeled value. No degradation was assumed when computing the models. Given that there are multiple sources of small margins of error in tape data and voltage tap measurement, linear regression, and modeling, these small-percent discrepancies can be considered less than reasonable experimental uncertainty.

The conclusion of this experiment is that no evidence was found of degradation in PIT VIPER cables caused by an extended solder process up to 2.5 hours in length, when tested at 77 K and in self-field. This paper therefore de-risks solder degradation in these conditions, both heat exposure and copper erosion, for SPARC cable magnets and many other potential applications.

References

[1] C. Sanabria *et al.*, "Development of a low ac loss and high current density high temperature superconducting cable," *Superconductor Science and Technology*, 2024. [Online]. Available: https://iopscience.iop.org/article/10.1088/1361-6668/ad7efc

[2] Z. Hartwig *et al.*, "Viper: an industrially scalable high-current high-temperature superconductor cable," *Superconductor Science and Technology*, October 2020. [Online]. Available: https://iopscience.iop.org/article/10.1088/1361-6668/abb8c0

[3] A. J. Creely, M. J. Greenwald, S. B. Ballinger, D. Brunner, J. Canik, J. Doody, T. Fülöp, D. T. Garnier, R. Granetz, T. K. Gray, and et al., "Overview of the sparc tokamak," *Journal of Plasma Physics*, vol. 86, no. 5, p. 865860502, 2020.

[4] A. Hubbard *et al.*, "Processes, systems and devices for metal filling of high temperature superconductor cables," U.S. Patent US20 240 290 520A1, April 2, 2024.

[5] J. Lu, Y. Xin, B. Jarvis, and H. Bai, "Oxygen out-diffusion in rebco coated conductor due to heating," *Superconductor Science and Technology*, vol. 34, no. 7, p. 075004, May 2021. [Online]. Available: https://dx.doi.org/10.1088/1361-6668/abfd0c

[6] M. Bonura, P. Cayado, K. Konstantopoulou, M. Alessandrini, and C. Senatore, "Heating-induced performance degradation of reba2cu3o7–x coated conductors: An oxygen out-diffusion scenario with two activation energies," *ACS Applied Electronic Materials*, vol. 4, no. 3, pp. 1318–1326, 2022. [Online]. Available: https://doi.org/10.1021/acsaelm.2c00065

[7] A. Hubbard *et al.*, "Superconducting cable comprising solder channel," Patent WO2 024 086 765A1, April 25, 2024.

[8] V. Bellos, I. Nalbantis, and G. Tsakiris, "Friction modeling of flood flow simulations," *Journal of Hydraulic Engineering*, vol. 144, no. 12, p. 04018073, 2018. [Online]. Available: https://ascelibrary.org/doi/abs/10.1061/%28ASCE%29HY.1943-7900.0001540

[9] A. Kaplan *et al.*, "Liquid nitrogen superconducting test facility at the mit plasma science and fusion center," *Submitted to IEEE Transactions on Applied Superconductivity*, September 2024.

[10] R. Granetz *et al.*, "Calculating the expected dc critical current, ic, in viper and corc cables and coils," September 2024, presented at ASC 2024, Salt Lake City UT. [Online]. Available: https://www.appliedsuperconductivity.org/asc2024

[11] N. Riva, R. S. Granetz, R. Vieira, A. Hubbard, A. T. Pfeiffer, P. Harris, C. Chamberlain, Z. S. Hartwig, A. Watterson, D. Anderson, and R. Volberg, "Development of the first non-planar rebco stellarator coil using viper cable," *Superconductor Science and Technology*, vol. 36, no. 10, p. 105001, aug 2023. [Online]. Available: https://dx.doi.org/10.1088/1361-6668/aced9d

[12] Z. S. Hartwig, R. F. Vieira, D. Dunn, T. Golfinopoulos, B. LaBombard, C. J. Lammi, P. C. Michael, S. Agabian, D. Arsenault, R. Barnett, M. Barry, L. Bartoszek, W. K. Beck, D. Bellofatto, D. Brunner, W. Burke, J. Burrows, W. Byford, C. Cauley, S. Chamberlain, D. Chavarria, J. Cheng, J. Chicarello, V. Diep, E. Dombrowski, J. Doody, R. Doos, B. Eberlin, J. Estrada, V. Fry, M. Fulton, S. Garberg, R. Granetz, A. Greenberg, M. Greenwald, S. Heller, A. E. Hubbard, E. Ihloff, J. H. Irby, M. Iverson, P. Jardin, D. Korsun, S. Kuznetsov, S. Lane-Walsh, R. Landry, R. Lations, R. Leccacorvi, M. Levine, G. Mackay, K. Metcalfe, K. Moazeni, J. Mota, T. Mouratidis, R. Mumgaard, J. Muncks, R. A. Murray, D. Nash, B. Nottingham, C. O'Shea, A. T. Pfeiffer, S. Z. Pierson, C. Purdy, A. Radovinsky, D. K. Ravikumar, V. Reyes, N. Riva, R. Rosati, M. Rowell, E. E. Salazar, F. Santoro, A. Sattarov, W. Saunders, P. Schweiger, S. Schweiger, M. Shepard, S. Shiraiwa, M. Silveira, F. Snowman, B. N. Sorbom, P. Stahle, K. Stevens, J. Stillerman, D. Tammana, T. L. Toland, D. Tracey, R. Turcotte, K. Uppalapati, M. Vernacchia, C. Vidal, E. Voirin, A. Warner, A. Watterson, D. G. Whyte, S. Wilcox, M. Wolf, B. Wood, L. Zhou, and A. Zhukovsky, "The sparc toroidal field model coil program," *IEEE Transactions on Applied Superconductivity*, vol. 34, no. 2, pp. 1–16, 2024.

[13] "Products - theva," accessed 2024-09-25. [Online]. Available: https://www.theva.com/products/

[14] N. M. Strickland, S. C. Wimbush, A. Pantoja, D. M. Pooke, M. Fee, V. Chamritskii, Z. Hartwig, J. Cheng, S. Garberg, and B. Sorbom, "Extended-performance "supercurrent" cryogen-free transport critical-current measurement system," *IEEE Transactions on Applied Superconductivity*, vol. 31, no. 5, pp. 1–5, 2021.

[15] J. Cheng, "Quantification of critical current prediction uncertainty in fusion cables introduced by variations in high temperature superconductor datasets," September 2023, presented at the 28th International Magnet Technology Conference, Aix-en-Provence, France. [Online]. Available: https://mt28.aoscongres.com